ANALYSIS OF VELOCITY FIELDS AND HEAT TRANSFER COEFFICIENTS OVER INCLINED INVERTED L-SHAPED BAFFLES IN A 3-D CHANNEL

by

Omolayo M. IKUMAPAYI[a], Noureddine KAID[b], Samia LARGUECH[c], Younes MENNI[b,d], Mustafa BAYRAM[e*], Abiodun BAYODE[a], Tin Tin TING[f,g], Salih OZER[h], and Erdinc VURAL[i]

[a] Department of Mechanical Engineering, Northwest University, Potchefstroom, South Africa
[b] Department of Mechanical Engineering, Institute of Technology,
University Center Salhi Ahmed Naama (Ctr. Univ. Naama), Naama, Algeria
[c] College of Engineering, Princess Nourah bint Abdulrahman University, Riyadh, Saudi Arabia
[d] College of Technical Engineering,
National University of Science and Technology, Dhi Qar, Iraq
[e] Department of Computer Engineering, Biruni University, Istanbul, Turkey
[f] Faculty of Data Science and Information Technology,
INTI International University, Nilai, Malaysia
[g] School of Information Technology, UNITAR International University, Selangor, Malaysia
[h] Mus Alparslan University, Mechanical Engineering, Mus, Turkiye
[i] Germencik Yamanturk Vocational School, Aydin Adnan Menderes University, Aydin, Turkiye

Original scientific paper
https://doi.org/10.2298/TSCI2504201I

Efficient thermal management in internal flow systems is critical for enhancing heat exchanger performance. This study investigates how variations in baffle inclination and flow rate affect flow behavior and heat transfer within a 3-D channel equipped with inverted L-shaped baffles. The flow is modeled under steady, laminar conditions with water as the working fluid. Results show that increasing flow velocity and adjusting baffle orientation generate complex 3-D flow structures, including vortex formation and secondary flows, which enhance fluid mixing and disrupt thermal boundary-layers. These effects lead to significant improvements in heat transfer, with the highest average heat transfer coefficient observed at the combination of greatest flow velocity and optimized baffle configuration, achieving up to 80% enhancement compared to less favorable set-ups. The findings demonstrate the synergistic influence of flow dynamics and baffle geometry in maximizing convective heat transfer, providing valuable insights for the design of more efficient thermal management systems.

Key words*: baffle inclination angle, momentum transport, numerical simulation, convective heat transfer, secondary flow structures*

Introduction

Baffle insertion is a proven passive technique for enhancing convective heat transfer in flow systems by disrupting thermal boundary-layers and promoting fluid mixing, thereby improving overall thermal performance. Numerous studies have demonstrated that the thermal

* Corresponding author, e-mail: mustafabayram@biruni.edu.tr

performance of baffled channels depends strongly on the geometry, orientation, spacing, flexibility, and material properties of the baffles. For instance, Yuan *et al.* [1] examined the performance of *U*-tube, *S*-channel, and baffle-guided solar collectors, revealing the significant role of flow guiding structures in boosting forced convection efficiency. Similarly, Sripattanapipat *et al.* [2] investigated *V*-shaped tapered baffles and their influence on turbulent flow topology and thermal mechanisms, while Salhi *et al.* [3] performed a 3-D analysis of corrugated channels embedded with baffles, achieving optimized thermohydraulic performance.

Inclined and perforated baffles were studied by Zhan *et al.* [4], who highlighted the impact of perforation patterns on pressure drop and heat transfer characteristics. Jamal *et al.* [5] explored variations in baffle length and placement, identifying optimal configurations for solar air channels. The innovative use of tilted grater-like baffles in two-pass channels was presented by Chang and Huang [6], who observed improvements in aerothermal behavior under different inclination angles. Alsabery *et al*. [7] introduced flexible baffles, offering a dynamic solution optimize local cooling performance for hot blocks in horizontal ducts.

The integration of inlet baffle structures was assessed by Du *et al*. [8] to counteract flow maldistribution and thermal non-uniformity in regenerative cooling applications. In photovoltaic systems, Lima-Tellez *et al.* [9] numerically evaluated the synergistic effect of baffles and nanofluids, emphasizing the enhancement of cooling uniformity. Jamal *et al*. [10] also demonstrated the value of novel-shaped baffles in managing turbulent heat transfer in solar air channels.

Hybrid and nanofluid applications in baffled geometries were further advanced by Ahamed *et al*. [11], who employed hybrid nanofluids in corrugated channels with *E*-shaped baffles, and Bouzennada *et al*. [12], who simulated heat transfer in micro-channels with elastic baffles. Discrete *XV*-shaped baffles were studied by Boonloi and Jedsadaratanachai [13], providing insights into laminar air-flow behavior and heat transfer optimization.

Beyond shape, Thanh [14] applied numerical and statistical methods (Taguchi analysis) to assess baffled channels for hot surface cooling. Phila *et al*. [15] examined the effect of notches on baffle performance, revealing enhanced flow channel interaction. Darbari and Ayani [16] implemented a two-phase Eulerian-Lagrangian model to capture the heat transfer and deposition behavior of nanofluids in baffled ducts, while Eiamsa-ard *et al*. [17] focused on aerothermal performance using perforated baffles in both experimental and numerical contexts.

Further experimental and numerical work by Eiamsa-ard *et al*. [18] elaborated on heat transfer distribution in perforated baffle channels. Mahmoud *et al*. [19] integrated ANN to evaluate the impact of hollow trapezoidal baffles on thermal-hydraulic behavior. Similarly, Feng *et al*. [20] conducted friction factor and heat transfer evaluations in triangular channels with trapezoidal baffles.

Promvonge and Skullong [21] enhanced the performance of solar receiver channels using flapped *V*-baffles, showing how localized flow disturbance improves convective efficiency. Hinged semi-circular baffles were proposed by Eiamsa-ard *et al*. [22], emphasizing their role in adaptive thermal control. El Habet *et al*. [23] assessed the combined effect of staggered and tilted perforated baffles, while Xu *et al.* [24] applied CFD-DEM modelling to explore fluid–particle dynamics in deduster channels with baffles.

This study investigates the combined effect of flow rate and baffle inclination angle on the hydrodynamic and thermal behavior of a 3-D rectangular channel with inclined inverted *L*-shaped obstacles. The hydrodynamic performance is assessed through detailed analysis of the velocity field, while the thermal performance is evaluated using both local and average heat transfer coefficients (HTC). By exploring a range of Reynolds number numbers and inclination

angles, the study aims to identify configurations that enhance flow structure and optimize convective heat transfer in channel-based thermal systems.

Geometric configuration and problem description

The investigated geometry consists of a 3-D rectangular channel engineered with embedded inverted *L*-shaped baffles inclined at angles of 30°, 45°, and 60°. These baffles are strategically affixed to both the top and bottom walls, while additional elements are placed along the channel's mid-height to enhance internal mixing and disrupt thermal stratification. This multi-level arrangement is purposefully designed to generate complex flow structures and augment surface heat transfer. The complete configuration, highlighting the spatial distribution and orientation of the baffles within the channel, is presented in fig. 1.

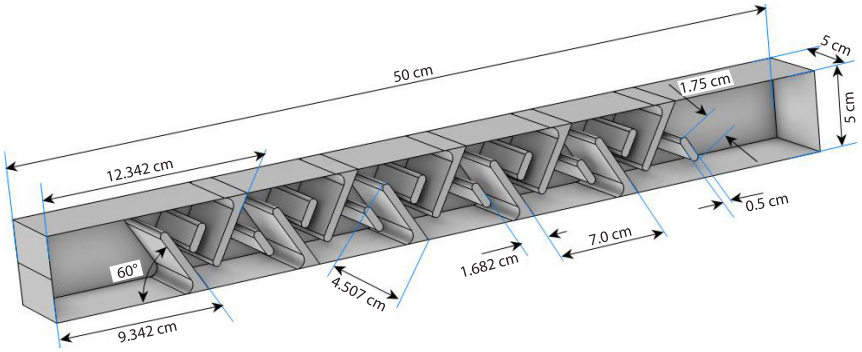

Figure 1. Flow domain with upper, lower, and central baffles

The inverted *L*-shaped baffles are designed to periodically disrupt the thermal and velocity boundary-layers. Their strategic placement and varying inclinations enhance the development of secondary flows, increase fluid-wall contact, and promote convective mixing near the heated surfaces, which are critical for improving heat transfer.

In this study, water serves as the working medium, characterized as an incompressible Newtonian fluid with uniform thermophysical properties. The flow regime is considered steady and laminar throughout the domain. Body forces, radiation, and buoyancy effects are neglected to isolate the influence of flow rate and baffle orientation on heat transfer behavior.

The fluid-flow and heat transfer within the computational domain are governed by the fundamental conservation laws of mass, momentum, and energy. Applying the previously stated assumptions, these governing equations are expressed in Cartesian co-ordinates.

Continuity equation:

$$\frac{\partial u}{\partial x}+\frac{\partial v}{\partial y}+\frac{\partial w}{\partial z}=0 \tag{1}$$

Navier-Stokes equation in the *x*-direction:

$$\rho\left(u\frac{\partial u}{\partial x}+v\frac{\partial u}{\partial y}+w\frac{\partial u}{\partial z}\right)=-\frac{\partial p}{\partial x}+\mu\left(\frac{\partial^2 u}{\partial x^2}+\frac{\partial^2 u}{\partial y^2}+\frac{\partial^2 u}{\partial z^2}\right) \tag{2}$$

Navier-Stokes equation in the *y*-direction:

$$\rho\left(u\frac{\partial v}{\partial x}+v\frac{\partial v}{\partial y}+w\frac{\partial v}{\partial z}\right)=-\frac{\partial p}{\partial y}+\mu\left(\frac{\partial^2 v}{\partial x^2}+\frac{\partial^2 v}{\partial y^2}+\frac{\partial^2 v}{\partial z^2}\right) \tag{3}$$

Navier-Stokes equation in the z-direction:

$$\rho\left(u\frac{\partial w}{\partial x}+v\frac{\partial w}{\partial y}+w\frac{\partial w}{\partial z}\right)=-\frac{\partial p}{\partial z}+\mu\left(\frac{\partial^2 w}{\partial x^2}+\frac{\partial^2 w}{\partial y^2}+\frac{\partial^2 w}{\partial z^2}\right) \tag{4}$$

Energy equation:

$$\rho C_p\left(u\frac{\partial T}{\partial x}+v\frac{\partial T}{\partial y}+w\frac{\partial T}{\partial z}\right)=k\left(\frac{\partial^2 T}{\partial x^2}+\frac{\partial^2 T}{\partial y^2}+\frac{\partial^2 T}{\partial z^2}\right) \tag{5}$$

where u, v, and w are velocity components, p – the pressure, ρ – the density, μ – theviscosity, k – the thermal conductivity, and C_p – the specific heat at constant pressure, are solved using the finite element method to accurately capture fluid-flow and heat transfer.

The computational model employs clearly defined hydrodynamic and thermal boundary conditions to simulate realistic flow and heat transfer behavior. At the inlet, a uniform velocity distribution and a constant fluid temperature are imposed to initiate a fully controlled flow regime. The outlet boundary is set to a zero-gradient condition for all variables, with the pressure fixed at atmospheric level, allowing the flow to exit freely without artificial disturbances. Along the channel walls, distinct thermal boundary conditions are applied. The lower wall serves as the heated surface and is subjected to no-slip and isothermal conditions, maintained at a constant temperature of 180 °C, thereby providing a continuous heat source to the fluid. In contrast, the upper wall is treated as no-slip and adiabatic, ensuring that while viscous interactions with the flow are captured, no heat transfer occurs across this boundary.

Results and discussion

A grid dependency analysis was performed to assess the sensitivity of the numerical results to mesh refinement and to identify an optimal mesh density that ensures accuracy without incurring excessive computational cost. Table 1 presents the average HTC and average Nusselt number for five progressively refined grids, ranging from 291836-1772164 elements.

Table 1. Mesh density impact on heat transfer characteristics at 60° inclination and Re = 600

Mesh elements	Average HTC [$Wm^{-2}K^{-1}$]	Average Nusselt number
291836	901.25	194.00
507000	941.16	245.58
871516	951.37	284.35
1485285	994.20	323.32
1772164	994.75	324.27

The results demonstrate a clear trend, both the average HTC and the Nusselt number increase with finer mesh resolution. The most notable variations occur between the coarsest grids. For instance, the Nusselt number increases from 194.00 for the 291836-element mesh to 284.35 for the 871516-element mesh, a significant jump indicating under-resolution in the coarser grids. However, as the grid is further refined beyond approximately 1.48 million elements, the changes in results become negligible. The difference in average HTC between the 1485285-element and 1772164-element grids is only 0.55 W/m^2K, and the corresponding increase in Nusselt number is just 0.95, representing a relative difference of approximately 0.3%. This small variation confirms that the solution has nearly reached grid independence. Considering the trade-off between computational efficiency and solution accuracy, the mesh

with 1485285 elements is selected for all subsequent simulations. This mesh offers sufficient resolution of flow and thermal gradients while maintaining manageable computational requirements.

The numerical model was validated by evaluating the pressure drop in a smooth channel and comparing the simulation results with the theoretical prediction. As shown in fig. 2, the computed pressure drop was obtained under the same conditions as those used in the theoretical formulation provided by Cengel and Cimbala [25], expressed:

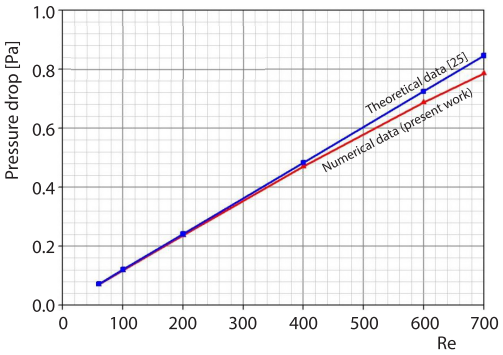

Figure 2. Comparison of numerical and theoretical pressure drop in a smooth channel

$$\Delta p = 32\frac{\mu L V_{\text{avg}}}{D^2} \tag{6}$$

where L is the channel length, V_{avg} – the average velocity, and D – the hydraulic diameter. The comparison reveals a good agreement between the present numerical results and the theoretical solution, confirming the accuracy and reliability of the computational model for predicting laminar flow pressure losses in smooth channels.

Figure 3 presents a comparative visualization of the velocity field within a channel equipped with inverted L-shaped baffles inclined at 30°, 45°, and 60°. The velocity field is illustrated for two distinct flow regimes: a low Reynolds number of 20, as shown in fig. 3(a), and a higher Reynolds number of 600, as shown in fig. 3(b).

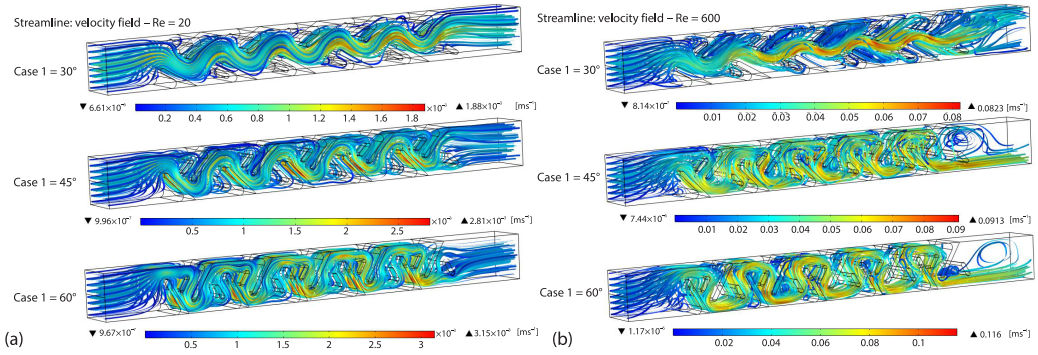

Figure 3. Velocity distributions at; (a) Re =20 and (b) Re = 600 with varying inclination angles

In fig. 3(a), corresponding to a Reynolds number of 20, the flow is dominated by viscous forces, and the velocity field remains largely stable and coherent. At a baffle inclination of 30°, the streamlines are mostly aligned in the streamwise direction, indicating minimal flow disturbance and weak re-circulation. The interaction between the fluid and the baffles is limited to localized regions near the baffle tips, and the core flow remains largely unaffected. As the baffle inclination increases to 45°, the flow exhibits stronger deviations from the axial direction, with moderate re-circulation zones forming downstream of the baffles. The increased angle introduces more pronounced streamline curvature and induces secondary flows that begin to extend deeper into the channel cross-section. When the inclination reaches 60°, the velocity field becomes significantly more disrupted. Large re-circulation

regions are visible behind the baffles, and the streamlines display strong deflection and swirling motion. The peak velocities are highest in this configuration, indicating enhanced flow acceleration around the baffle edges and improved interaction with the heated wall. These observations suggest that at low Reynolds numbers, increasing the baffle angle promotes stronger flow redirection and mixing, although the extent of disruption remains constrained by the dominance of viscous effects.

In contrast, fig. 3(b) illustrates the velocity field at a Reynolds number of 600, where inertial effects dominate and the flow structure becomes significantly more complex and 3-D. At a baffle inclination of 30°, the streamlines begin to deviate and exhibit signs of re-circulation, particularly in the wake regions behind the baffles. However, the overall flow disruption remains modest, and the core flow retains a relatively strong alignment along the axial direction of the channel. As the baffle inclination increases to 45°, the velocity field demonstrates a substantial increase in flow complexity. Multiple vortex structures emerge downstream of the baffles, and the interaction between adjacent flow layers intensifies. The inclusion of centrally positioned baffles further contributes to the development of cross-stream motion and vertical flow redistribution. This leads to more uniform mixing throughout the channel height and enhances the penetration of high momentum fluid into near-wall regions. At an inclination of 60°, the flow undergoes the most pronounced transformation. The streamlines display chaotic, swirling patterns and the formation of large, coherent vortical structures becomes evident. Flow impingement on the heated walls and reattachment downstream emerge as dominant features, indicating the generation of strong secondary flows. In this configuration, the velocity magnitudes reach their peak values, confirming a significant enhancement in momentum transport and convective mixing.

Comparing figs. 3(a) and 3(b), it is evident that both the Reynolds number and the baffle inclination play critical roles in shaping the velocity field. At lower Reynolds numbers, the flow remains largely laminar with localized enhancements near the baffles. As the Reynolds number increases, the flow becomes increasingly energetic and 3-D, with the baffle geometry exerting a greater influence on flow separation and re-circulation. The 60° configuration consistently shows the highest level of flow disruption and secondary flow formation across both flow regimes. These characteristics are beneficial for convective heat transfer, as they promote stronger wall-fluid interactions and periodic boundary-layer renewal. The increased flow disturbance and enhanced mixing observed in the 60° cases suggest a superior capacity for thermal performance, a conclusion further supported by the heat transfer data presented in figs. 4 and 5.

Figure 4 illustrates the influence of flow rate, represented by Reynolds number, and baffle inclination angle on the local HTC distribution along the channel length. The results highlight a clear dependency of thermal performance on both parameters. At a low Reynolds number of 20, as shown in fig. 4(a), where the flow is strongly governed by viscous forces, the overall enhancement in heat transfer is modest across all inclination angles. The 30° baffles generate only mild undulations in the local HTC, reflecting limited disruption of the thermal boundary-layer. Increasing the inclination 45° leads to more distinct periodic peaks, indicating localized enhancement caused by moderate flow separation and reattachment. The 60° inclination results in more pronounced peaks even at this low flow rate, suggesting that steeper baffles are more effective in disturbing the boundary-layer and promoting localized convective exchange. However, the overall impact remains constrained due to the low inertial energy of the flow.

As the Reynolds number increases to 600, as reported in fig. 4(b), the effect of flow inertia becomes dominant, amplifying the influence of baffle geometry. At this higher flow

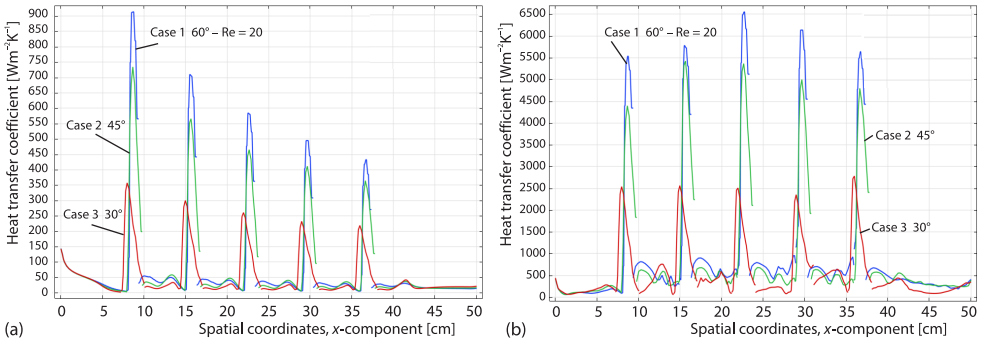

Figure 4. Local HTC along the channel at; (a) Re = 20 and (b) Re = 600 for various inclinations

rate, the 30° configuration exhibits moderate heat transfer enhancement, while the 45° angle produces significantly higher and more frequent peaks in the local HTC, driven by stronger vortex formation and improved fluid-wall interaction. The most substantial enhancement is observed with the 60° baffles, which generate sharp, periodic spikes in the heat transfer profile due to vigorous secondary flows, vortex impingement, and repeated disruption of the thermal boundary-layer. These findings demonstrate that increasing the flow rate enhances the overall convective performance, but the degree of enhancement is strongly dependent on the inclination angle. Baffles with greater inclination angles consistently outperform shallower ones, particularly under high Reynolds number conditions, where the combined effect of flow momentum and geometric forcing leads to intensified mixing, boundary-layer thinning, and ultimately superior heat transfer characteristics.

At a low Reynolds number of 20, as shown in fig. 5, increasing the baffle inclination from 30° (54.29 W/m^{2}K) to 60° (84.24 W/m^{2}K) improves the average HTC by about 55%. As the Reynolds number increases from 20-600, the average HTC rises dramatically across all inclinations: from 54.29-550.64 W/m^{2}K at 30° (an increase of approximately 915%), from 79.71-923.70 W/m^{2}K at 45° (about 1058%), and from 84.24-994.07 W/m^{2}K at 60° (nearly 1080%). At the highest Re number of 600, increasing the baffle angle from 30-60° boosts the average HTC by around 80%. These values clearly indicate that the combination of high flow rate and steep baffle inclination produces the optimal heat transfer performance.

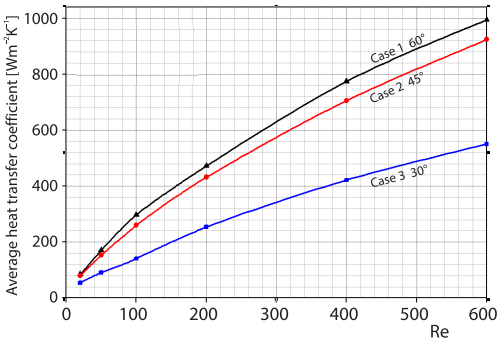

Figure 5. Average HTC for various baffle inclination angles and Reynolds numbers

Conclusion

The numerical investigation confirms that both Reynolds number and baffle inclination angle play crucial roles in shaping flow dynamics and thermal performance within baffled rectangular channels. Increasing Reynolds number from 20-600 substantially enhances the average HTC due to strengthened inertial forces, flow mixing, and boundary-layer disruption. Among the tested geometries, baffles inclined at 60° consistently provide superior average HTC, outperforming 45° and 30° inclinations by up to 80% at higher flow rates. Velocity field analyses demonstrate that higher inclinations and flow rates promote complex 3-D vortices and

secondary flows, which are responsible for improved convective mixing near heated surfaces. The optimal configuration identified at Re = 600 and 60° inclination achieves the highest average HTC of approximately 994.07 W/m^{2}K, underscoring the effectiveness of steep baffles combined with high flow momentum. This study highlights the importance of carefully tuning baffle geometry and flow conditions to maximize heat exchanger efficiency, providing practical guidelines for engineering applications requiring enhanced heat transfer.

Acknowledgment

Princess Nourah bint Abdulrahman University Researchers Supporting Project number (PNURSP2025R826), Princess Nourah bint Abdulrahman University, Riyadh, Saudi Arabia.

References

[1] Yuan, G., *et al.*, Enhancing Forced Convection Solar Collector Efficiency Through Structural Optimization: A Comparative Study of U-Tube, Flow-Guiding Baffle and S-Channel Configurations, *Results in Engineering*, *27* (2025), 106354
[2] Sripattanapipat, S., *et al*., Flow Topology and Thermal Mechanism in Turbulent Channel Flow with Tapered V-Shaped Baffles, *Case Studies in Thermal Engineering*, *73* (2025), 106610
[3] Salhi, J. E., *et al.*, The 3-D Analysis of Thermohydraulic Performance in Corrugated Channels with Embedded Baffles: Optimization of Heat Transfer and Energy Efficiency, *Case Studies in Thermal Engineering*, *69* (2025), 106019
[4] Zhan, Y., *et al*., Numerical Investigation of Flow and Heat Transfer Characteristics in a Rectangular Channel with Perforated Inclined Baffle, *International Communications in Heat and Mass Transfer*, *164* (2025), 108941
[5] Jamal, I., *et al*., Numerical Analysis of the Effect of Baffle Length and Arrangement on the Thermal Performance of Solar Air Channels, *International Communications in Heat and Mass Transfe*r, *161* (2025), 108458
[6] Chang, S. W., Huang, P. N., Aerothermal Performance of Two-Pass Channel with Tilted Grater-Baffles, *Chemical Engineering and Processing-Process Intensification*, *205* (2024), 109969
[7] Alsabery, A. I., *et al*., Enhancement of Cooling Process of Hot Blocks Mounted Inside a Horizontal Channel Using Flexible Baffles – Alternative Arrangement, *International Journal of Thermofluids*, *23* (2024), 100805
[8] Du, W., Flow Maldistribution and Heat Transfer Non-Uniformity with an Inlet Baffle Structure in Regenerative Cooling Channels, *Applied Thermal Engineering*, *258* (2025), 124619
[9] Lima-Tellez, T., *et al*., Numerical Study of the Thermal Performance of a Single-Channel Cooling PV system Using Baffles and Different Nanofluids, *Heliyon*, *10* (2024), 15, e35413
[10] Jamal, I., *et al*., Enhancing Performance in Solar Air Channels: A Numerical Analysis of Turbulent Flow and Heat Transfer with Novel Shaped Baffles, *Applied Thermal Engineering*, *251* (2024), 123561
[11] Ahamed, R., *et al*., Thermal-Hydraulic Performance and Flow Phenomenon Evaluation of a Curved Trapezoidal Corrugated Channel with E-Shaped Baffles Implementing Hybrid Nanofluid, *Heliyon*, *10* (2024), 7, e28698
[12] Bouzennada, T., *et al*., Numerical Study on Nanofluid Heat Transfer and Fluid-Flow Within a Micro-Channel Equipped with An Elastic Baffle, *Case Studies in Thermal Engineering*, *56* (2024), 104247
[13] Boonloi, A., Jedsadaratanachai, W., Numerical Investigations of Laminar Air-flow and Heat Transfer Characteristics in a Square Channel Inserted with Discrete XV Baffles (XVB), *Frontiers in Heat and Mass Transfer*, *21* (2023), pp. 317-336
[14] Thanh, L. N., The influence of Baffled Channel for Cooling Hot Surface: Numerical Simulation and Taguchi analysis, *Case Studies in Thermal Engineering*, *52* (2023), 103646
[15] Phila, A., *et al*., Influence of Notched Baffles on Aerothermal Performance Behaviors in a Channel, *Case Studies in Thermal Engineering*, *47* (2023), 103070
[16] Darbari, B., Ayani, M. B., Heat Transfer and Deposition Analysis of CuO-Water Nanofluid Inside a Baffled Channel: Two-Phase Eulerian-Lagrangian Method, *Journal of the Taiwan Institute of Chemical Engineers*, *148* (2023), 104827
[17] Eiamsa-Ard, S., *et al*., Thermal Evaluation of Flow Channels with Perforated-Baffles, *Energy Reports*, *9* (2023), pp. 525-532

[18] Eiamsa-Ard, S., *et al*., Heat Transfer Distribution and Flow Characteristics in a Channel with Perforated-Baffles, *Energy Reports*, *8* (2022), Suppl. 15, pp. S420-S426
[19] Mahmoud, I. A., *et al*., Hollow trapezoidal baffles in a Rectangular Channel: Thermal/Hydraulic Assessment with ANN Numerical Approach, *International Communications in Heat and Mass Transfer*, *139* (2022), 106505
[20] Feng, C. N., *et al.*, Friction Factor and Heat Transfer Evaluation of Cross-Corrugated Triangular Flow Channels with Trapezoidal Baffles, *Energy and Buildings*, *257* (2022), 111816
[21] Promvonge, P., Skullong, S., Thermal-Hydraulic Performance Enhancement of Solar Receiver Channel by flapped V-Baffles, *Chemical Engineering Research and Design*, *182* (2022), June, pp. 87-97
[22] Eiamsa-Ard, S., *et al*., Enhanced Heat Transfer Mechanism and Flow Topology of an Channel Contained With Semi-Circular Hinged V-Shaped Baffles, *International Journal of Thermal Sciences*, *177* (2022), 107577
[23] El Habet, M. A., *et al*., The Effect of Using Staggered and Partially Tilted Perforated Baffles on Heat T*ransfer and Flow Characteristics in a Rectangular Channel, International Journal of Thermal Scienc*es, *174* (2022), 107422
[24] Xu, H., *et al*., The CFD-DEM Study of Fluid-Flow and Particle Behaviors in a Baffled Deduster Channel, *Chemical Engineering Research and Design*, *176* (2021), Dec., pp. 123-133
[25] Cengal, Y. A., Cimbala, J. M., *Fluid Mechanics: Fundamentals and Applications*, 4th ed., McGraw-Hill Education, 2 Penn Plaza, New York, USA, 2017, 10121

Paper submitted: March 15, 2025
Paper revised: June 14, 2025
Paper accepted: July 28, 202